

Photothermal response enhancement in heterogeneous plasmon-resonant nanoparticle trimers

Seyfollah Toroghi and Pieter G. Kik*

CREOL, The College of Optics and Photonics, University of Central Florida, 4000 Central Florida Blvd., Orlando, Florida 32816, USA

(Received 12 February 2014; revised manuscript received 30 September 2014; published 11 November 2014)

The optical response of heterogeneous plasmonic trimer structures composed of a silver nanoparticle dimer and a central gold nanoparticle is investigated analytically and numerically. The plasmon resonance of the silver dimer is controlled through near-field coupling, resulting in plasmon resonance frequency matching of the silver dimer and gold monomer. This coupling condition makes it possible to increase the energy dissipation per unit volume in the gold particle by over two orders of magnitude compared to a single-particle system. It is predicted that pulsed illumination of a trimer consisting of two 80-nm-diameter silver particles and a 10-nm-diameter central gold particle can raise the gold particle temperature by 100 K using a pump fluence as low as 20 nJ/mm² at a wavelength of 530 nm. This finding may have practical applications in photothermal therapy, fast thermal nonlinear optical modulation, and could enable new fundamental thermal studies at picosecond time scales.

DOI: [10.1103/PhysRevB.90.205414](https://doi.org/10.1103/PhysRevB.90.205414)

PACS number(s): 78.67.Bf, 65.80.-g, 73.20.Mf, 78.20.nb

I. INTRODUCTION

Heat generation in metallic nanoparticles under optical illumination has recently attracted enormous interest, having found applications in photothermal therapy [1–5], drug delivery [6–8], photothermal imaging [9–11], optoacoustic imaging [12,13], bubble formation for nanosurgery [14–18] and liquid purification [19,20], material growth [21], nanowelding [22,23], heat-assisted magnetic recording [24], and photothermally controlled fluidics [25,26]. In metallic nanoparticles, plasmon resonances lead to enhanced optical absorption, accompanied by heating of the free electron gas through electron-electron scattering on a time scale of ~ 100 fs [27] and resulting in an ultrafast nonlinear optical response [28–31]. Subsequently the electron gas exchanges energy with the metal lattice through electron-phonon scattering on a time scale of 2–3 picoseconds bringing the electronic and vibrational temperature of the particle in equilibrium [32]. This is followed by heat transfer to the surrounding medium on a ~ 100 ps time scale. The combination of plasmon enhanced optical absorption and rapid heat dissipation make metallic nanostructures an attractive candidate for a wide range of photothermal applications.

Given the broad applicability of the plasmonic photothermal effect, it is of interest to find ways of maximizing the attainable temperature change for a given optical irradiance. In the present article we achieve this by using a compositionally heterogeneous trimer structure consisting of a relatively high-volume plasmon-resonant dimer with a small-volume plasmon-resonant monomer. The optical properties of compositionally heterogeneous plasmonic structures have been previously investigated theoretically [33,34], however, these studies did not achieve strongly coupled resonances due to a significant resonance mismatch between the different nanospheres. Related experimental studies in the context of gas sensing [35,36] and signal routing [37,38] demonstrated the benefit of combining different materials into coupled systems, but did not achieve large field enhancement factors due to either the presence of a resonance frequency mismatch of the

plasmonic elements or the introduction of large damping by one of the materials used (Pd). In contrast to these studies, we demonstrate that a plasmonic trimer composed of a silver dimer and a gold monomer can exhibit strong resonant interactions between the different materials, enabling the achievement of large field enhancement and the generation of a temperature change that exceeds that of isolated gold nanoparticles by over two orders of magnitude. The presented approach uses elements of the plasmonic nanolens introduced by Li *et al.* [39], which relied on cascaded resonances between nanospheres with identical composition in order to achieve large field enhancement factors. In the present study we show that judiciously chosen near-field induced resonance shifts can be used to achieve cascaded plasmon resonances in *compositionally heterogeneous* nanosphere structures, something which could not be achieved with the geometry introduced by Li *et al.* The physical principle that makes this possible is illustrated in a point-dipole coupling model, and confirmed by numerical simulations of an experimentally realistic nanoparticle trimer. The general approach presented here can be extended to a broad range of nanoparticle sizes and compositions, and offers new opportunities for optimizing plasmon enhanced phenomena.

II. THEORY

To optimize the photothermal response in plasmonic nanostructures we monitor the ratio of the absorption cross section σ_{abs} to the nanoparticle volume V_{NP} . In metallic nanoparticles the temperature change immediately after short pulse illumination is given by $\Delta T(K) = \sigma_{\text{abs}}\phi / (\rho_{\text{NP}}c_{\text{NP}}V_{\text{NP}})$ with $\phi(\text{J m}^{-2})$ the optical fluence of the pulse, $\rho_{\text{NP}}(\text{kg m}^{-3})$ the density of the particle, and $c_{\text{NP}}(\text{J kg}^{-1} \text{K}^{-1})$ the specific heat capacity of the particle, assuming that the specific heat is approximately temperature independent. Note that ΔT depends only on material properties and the relative absorption coefficient $\sigma_{\text{abs}}/V_{\text{NP}}$. For spherical metallic nanoparticles in the quasielectrostatic limit the relative absorption coefficient becomes size independent and approximately peaks at the localized plasmon resonance frequency ω_{LSP} with a magnitude given by

$$\left(\frac{\sigma_{\text{abs}}}{V_{\text{NP}}}\right)_{\omega_{\text{LSP}}} = 9 \frac{\omega_{\text{LSP}}}{c} \frac{n_h^3}{\epsilon''_{\text{NP}}}, \quad (1)$$

*Also at Physics Department, University of Central Florida; kik@creol.ucf.edu

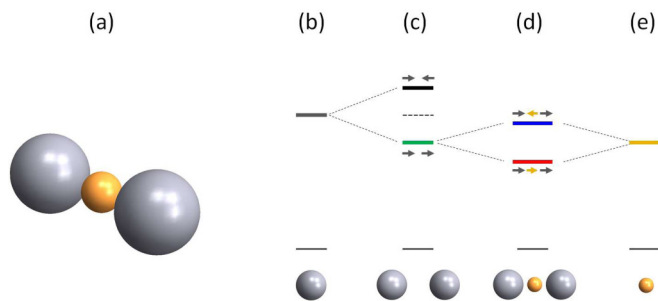


FIG. 1. (Color online) (a) Schematic of a heterogeneous Ag-Au-Ag trimer. Energy diagrams showing (b) the dipolar plasmon mode of an isolated silver nanoparticle, (c) the bonding (green) and antibonding (black) resonance modes of a silver dimer, (d) the bonding (red) and antibonding (blue) modes of an Ag-Au-Ag nanosphere trimer, and (e) the dipolar plasmon resonance mode of an isolated gold nanoparticle.

where c is the speed of light in vacuum, n_h is the refractive index of the host, and $\varepsilon_{\text{NP}}''$ is the imaginary part of the dielectric function of the metal particle at ω_{LSP} . For gold nanoparticles in an aqueous host the peak relative absorption coefficient is $\sim 0.083 \text{ nm}^{-1}$ at a wavelength of 515 nm, leading to a $\Delta T/\varphi = 33 \text{ K}/(\mu\text{J}/\text{mm}^2)$. To achieve maximum nanoparticle heating for a given pulse energy this relative absorption must be optimized. Here we use the strong optical field in the gap of a dimer composed of a high-plasma-frequency metal to drive the plasmon resonance of a smaller nanoparticle composed of a material with a lower plasma frequency.

Figure 1(a) shows an illustration of the type of heterogeneous trimer structure under investigation. The trimer is bimetallic, and consists of a gold nanoparticle located between two silver nanoparticles. This system supports various coupled plasmon resonances which can be understood in terms of hybridization of modes of the separate elements in the structure, as shown schematically in Figs. 1(b)–1(e). Figures 1(b) and 1(e) show energy level diagrams corresponding to the dipolar plasmon resonance energies of isolated silver and gold nanospheres in water ($n = 1.33$) which lie at 3.24 and 2.41 eV, respectively. Due to the large mismatch between these energies, Au and Ag nanoparticles are not expected to show strong plasmonic interaction. Figure 1(c) shows the energies of coupled dipolar plasmon resonances on a silver nanosphere dimer for modes polarized along the dimer axis. Near-field interactions between the closely spaced silver nanoparticles induce polarization-dependent mode splitting, resulting in the development of a low-energy bonding mode where electrons in both particles oscillate in phase, and a high-energy antibonding mode where the electrons in each particle oscillate in antiphase [40]. For sufficiently strong interparticle interaction (i.e., at small spacing), the energy of the lowest order silver dimer bonding mode may approach the resonance energy of an isolated gold nanoparticle, as indicated schematically by the green horizontal line in Fig. 1(c). This type of near-field induced resonance shift of the silver dimer thus provides a method for achieving strong coupling between plasmon resonances in heterogeneous particle systems. Figure 1(d) shows two anticipated coupled resonances when a trimer is composed of a gold nanosphere and the silver dimer from

Fig. 1(c). Coupling between the bonding mode of the silver dimer and the dipolar resonance of the gold monomer is expected to lead to the development of hybridized modes, exhibiting a low-energy bonding mode where the dipole moment of all particles oscillates approximately in phase, and a higher-energy antibonding mode where the Au dipole moment and Ag dipole moment oscillate in antiphase, as indicated schematically by the arrows in Fig. 1(d). This type of coupling can produce large field enhancement factors and consequently a large concentration of energy dissipation.

To investigate the evolution of hybridized plasmon modes as a function of particle polarizability in heterogeneous trimer structures we first consider a point-dipole interaction model, similar to the approach taken in Ref. [41]. Each particle in the trimer is modeled as a point dipole with polarizability $\alpha_i = 3\varepsilon_0\varepsilon_h V_i(\varepsilon_i - \varepsilon_h)/(\varepsilon_i + 2\varepsilon_h)$ where ε_0 is the vacuum permittivity, V_i is the volume of nanoparticle i , and ε_i and ε_h are the dielectric function of particle i and the host, respectively. The dipole moment of particle i at location \mathbf{r}_i is given by $\mathbf{p}_i = \alpha_i \mathbf{E}_{\text{loc}}(\mathbf{r}_i)$, where $\mathbf{E}_{\text{loc}}(\mathbf{r}_i) = \mathbf{E}_{\text{inc}}(\mathbf{r}_i) - \sum \mathbf{A}_{ij} \mathbf{p}_j$ represents the local field experienced by particle i due to the incident electric field $\mathbf{E}_{\text{inc}}(\mathbf{r}_i)$ and contributions from neighboring dipoles j , with \mathbf{A}_{ij} the dipole-dipole interaction matrix between dipoles i and j . For a centrosymmetric linear trimer structure consisting of identical outer particles 1 and 3 and a central particle 2 excited with an electric field polarized along the trimer axis we have $\alpha_1 = \alpha_3$ and $p_1 = p_3$, and scalar matrix elements A_{ij} given by

$$A_{ij} = \frac{e^{ikd_{ij}}}{2\pi\varepsilon_0\varepsilon_h} \left(\frac{ik}{d_{ij}^2} - \frac{1}{d_{ij}^3} \right), \quad (2)$$

where d_{ij} is the center-to-center separation between particles i and j , and k is the wave vector in the host medium. Solving for the dipole moment p_2 and converting this to the internal field enhancement factor $E_{\text{in},2}$ of particle 2 using the field enhancement factor $g_{\text{in},2} = E_{\text{in},2}/E_{\text{loc}}(r_2) = 3\varepsilon_h/(\varepsilon_2 + 2\varepsilon_h)$ we find

$$\frac{E_{\text{in},2}}{E_{\text{inc}}} = \frac{1 + \alpha_1 A_{13} - 2\alpha_1 A_{12}}{1 + \alpha_1 A_{13} - 2\alpha_1 \alpha_2 A_{12}^2} g_{\text{in},2}. \quad (3)$$

III. RESULTS AND DISCUSSION

A. Point dipole model

Equation (3) is used to investigate mode hybridization and field enhancement factors in trimers consisting of outer particles described by a Drude dielectric response with a high plasma frequency $\omega_{pA} = 9 \times 10^{15} \text{ rad/s}$ and a central particle with a lower plasma frequency $\omega_{pB} = 8 \times 10^{15} \text{ rad/s}$, embedded in an aqueous host with $\varepsilon_h = 1.77$. Both materials are assumed to have an electron scattering rate of $\gamma_A = \gamma_B = 10^{14} \text{ s}^{-1}$, similar to that of noble metals. Figure 2(a) shows the evolution of the obtained plasmon resonance energies of the symmetric bonding mode [all dipoles in phase (red line)] and the antibonding mode [central dipole in antiphase with outer particles (blue line)] in trimers where the diameter of the outer particles is set to 80 nm and the diameter of the central particle D_2 is varied from 0 to 80 nm, while the edge-to-edge spacing is held fixed at 5 nm. The corresponding separation d_{13} between the outer particles is shown on the top axis. For comparison,

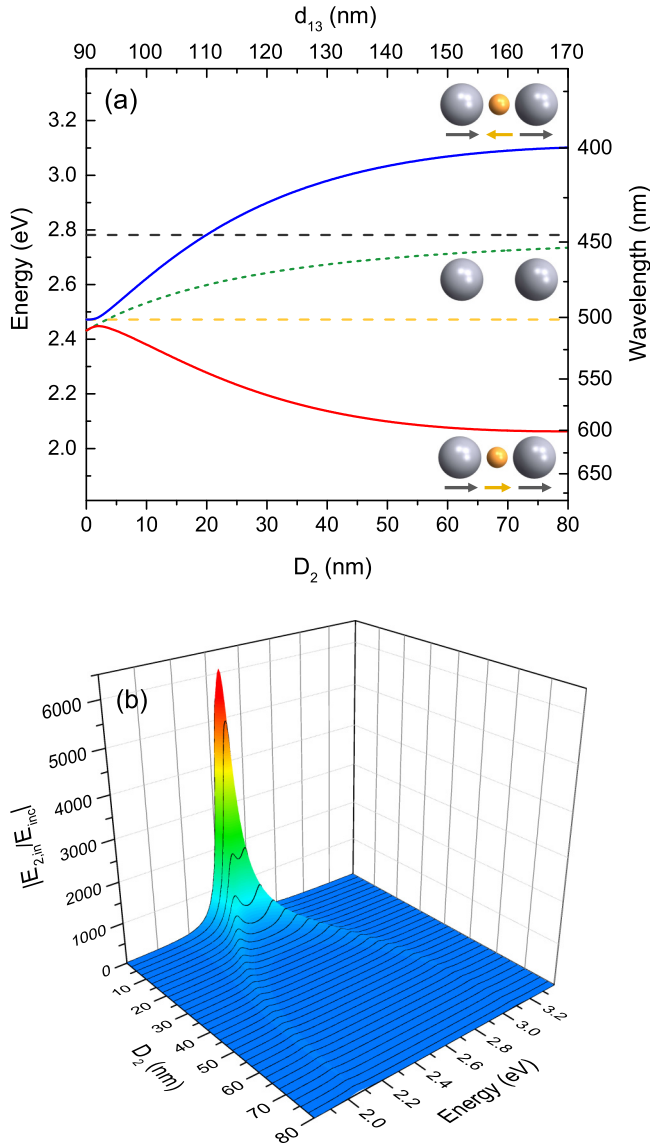


FIG. 2. (Color online) (a) Plasmon resonance energies of a heterogeneous nanoparticle trimer as a function of the central particle diameter D_2 , as well as the resonance energies of isolated outer (black dashed line) and central nanoparticles (gold dashed line), and of the bonding mode of an isolated dimer (green dotted line). (b) Corresponding internal field enhancement spectra of the central nanoparticle as a function of its diameter D_2 .

the bonding resonance of the equivalent isolated dimers is included (green dotted line, top axis), as well as the resonance energies of isolated outer and central particles (black and gold dashed horizontal lines, respectively). The presence of a large central particle in the trimer is seen to cause significant mode splitting between the bonding and antibonding modes due to the large polarizability of the central particle. As the diameter of the central particle is reduced, the influence of the central particle on the trimer resonances diminishes, causing the mode splitting to reduce while both resonances approach the resonance energy of the isolated dimer. Note that for a central particle diameter of 3.45 nm, the small physical separation between outer particles causes the dimer resonance to match

that of an isolated central particle [level alignment as in Fig. 1(c)], while at the same time the small polarizability of the central particle leads to relatively small mode splitting between the bonding and antibonding modes. This condition leads to the development of large field enhancement, as shown below.

Figure 2(b) shows the magnitude of the internal electric field enhancement factor in the central particle for the same parameters as used in Fig. 2(a). At large volume of the central particle, only moderate field enhancement values of the order of 30 are observed for both the bonding and the antibonding modes. As the volume of the central particle is reduced, the mode splitting decreases and the field enhancement rises dramatically. This can be understood by noting that for small central particle size, the dimer resonance matches the resonance of the central particle, while the central particle has relatively little effect on the dimer resonance due to its small volume. Under these conditions the dimer acts as an excitation source for the smaller central particle, which in turn produces its own field enhancement. This effect is analogous to the plasmonic nanolens [39], but extended to nanospheres with varying composition.

B. Numerical simulations

To evaluate the feasibility of optimizing field enhancement and the photothermal response in realistic heterogeneous trimer structures we simulated the electric field distribution in Ag-Au-Ag trimers using the three-dimensional frequency domain finite integration technique [42] taking into account literature dielectric functions for silver [43] and gold [44]. This method takes into account radiative losses and allows for multipolar plasmons, aspects that are not included in the point-dipole model discussed above. The silver nanoparticle diameter and edge-to-edge spacing were held at 80 and 5 nm, while the gold nanoparticle diameter was varied between 10 and 80 nm. The trimer is oriented along the x axis and excited using an x -polarized plane wave with field amplitude E_0 and a wave vector normal to the dimer axis. Based on the numerically simulated electric field distributions, the material-specific relative absorption coefficient σ_i/V_i can be extracted, where σ_i represents the ratio of the power dissipated in particle i to the incident irradiance on the trimer, leading to

$$\frac{\sigma_i}{V_i} = \frac{\omega \epsilon_i''}{V_i n_h c} \int_{V_i} \frac{E^*(r) \cdot E(r)}{E_0^2} dr. \quad (4)$$

Figure 3(a) shows the thus obtained gold-related relative absorption for heterogeneous trimers with three different gold nanosphere sizes (solid lines), the corresponding result for the isolated gold nanoparticles at these sizes (dotted lines), and the silver-related relative absorption of isolated silver dimers at the same interparticle spacings (dashed lines). The relative Au-related absorption of the trimer with an 80-nm-diameter central particle (red solid line) shows a peak at 495 nm and a shoulder at ~ 675 nm, indicative of the previously discussed antibonding and bonding modes. At this Au particle size, the equivalent Ag dimer shows a resonance at 445 nm, and does not match the resonance frequency of the Au nanoparticle. The highest relative absorption of the Au nanoparticle in this trimer is ~ 0.08 (nm^{-1}) compared to 0.07 (nm^{-1}) of the isolated gold particle at this size. As the gold diameter in the trimer is

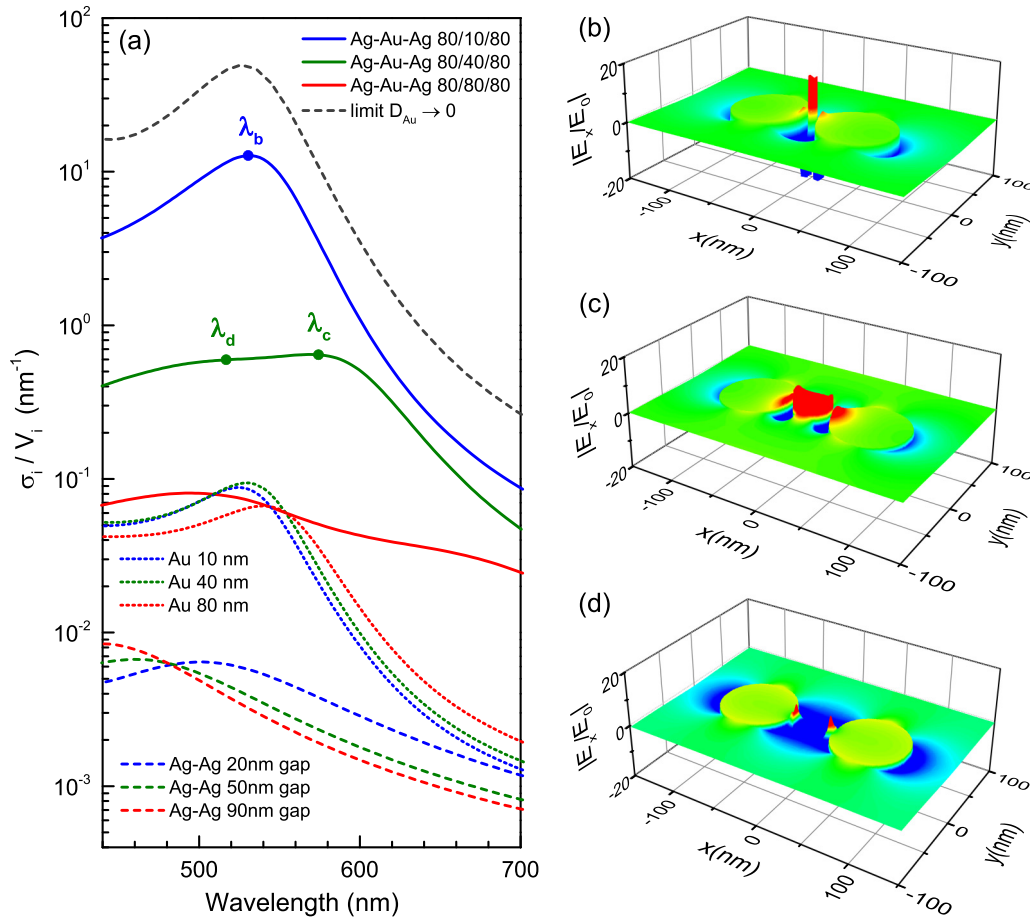


FIG. 3. (Color online) (a) Gold-related relative absorption coefficient (solid lines) for nanoparticle trimers consisting of 80-nm-diameter outer silver nanoparticles and a central gold nanoparticle with a diameter of 80 nm (red line), 40 nm (green line), and 10 nm (blue line), respectively, as well as the corresponding results for isolated gold particles with these same dimensions (dotted lines), and the silver-related relative absorption for the corresponding isolated silver dimers (dashed lines). (b) Snapshot of the electric field distribution E_x corresponding to the case labeled λ_b , (c) corresponding to the case labeled λ_c , and (d) corresponding to the case labeled λ_d .

reduced to 40 nm, the relative absorption is seen to increase by as much as an order of magnitude. The corresponding results for the isolated gold particle increase by only a factor ~ 1.4 for the same size reduction. Note that the Ag dimer resonance (green dashed line) moves closer to the Au nanoparticle resonance. The relative absorption spectrum of this trimer shows a peak at long wavelength and a shoulder at short wavelength. Two representative field snapshots corresponding to wavelengths $\lambda_c = 570$ nm and $\lambda_d = 510$ nm are shown in Figs. 3(c) and 3(d), respectively. At low frequency (λ_c) the field inside the silver particles and the gold particle are both seen to be positive, indicative of a bonding mode. At high frequency (λ_d) on the other hand, the field in the silver particles can be seen to be positive, while the field inside the gold nanoparticle is negative, indicative of an antibonding mode. As the gold particle diameter is further reduced to 10 nm, the maximum relative absorption increases by another order of magnitude (blue solid line) peaking at $\lambda_b = 530$ nm. A snapshot of the corresponding electric field distribution at λ_b is shown in Fig. 3(b). Large electric field strength is observed inside the gold nanoparticle, resulting in the desired larger energy dissipation per unit volume. Note that the equivalent Ag dimer resonance now occurs at 502 nm, close to the Au nanoparticle

resonance. Continued size reduction (not shown) of the gold particle diameter D_{Au} leads to a gradual convergence to the limiting case of $(\sigma/V)_{\text{Au}} = (\omega \epsilon''_{\text{Au}} / n_h c) |g_{\text{gap}}(\omega) g_{\text{in,Au}}(\omega)|^2$ where $g_{\text{in,Au}}$ is the theoretical internal field enhancement factor for a gold nanosphere in the quasielectrostatic limit, and g_{gap} represents the simulated field enhancement at the gap center of an isolated silver dimer with a 10 nm gap, as shown by the gray dashed line in Fig. 3(a). In our prior work on single-composition dimers [41], we labeled this regime “multiplicative cascading,” referring to the fact that the field enhancement is well described by the product of the enhancement factors provided by the individual elements of the structure. In this limit, the relative absorption of Au nanoparticles in the trimer structure exceeds that of isolated Au particles of the same size by a factor 470. Comparing the peak response of the trimer with a 10-nm-diameter Au particle with the previously calculated thermal response of $\Delta T/\varphi = 33 \text{ K}/(\mu\text{J}/\text{mm}^2)$ for isolated Au nanoparticles, the results in Fig. 3 indicate that a pulse fluence as small as $20 \text{ nJ}/\text{mm}^2$ at 530 nm could produce a temperature change of 100 K in these trimers.

The results presented above demonstrate that the relative absorption coefficient of gold nanoparticles can be enhanced

by orders of magnitude using coupled resonances in heterogeneous few-particle structures. This optimized absorption enables the achievement of large temperature changes, which could lead to significantly enhanced thermal nonlinear optical response of the gold nanoparticle. In addition, the small size of the gold particles and the highly concentrated heat deposition is anticipated to enable rapid heating and cooling of the gold nanoparticle under pulsed illumination in an aqueous environment (relaxation time of hundreds of picoseconds [45]), implying that any thermo-optic nonlinearities in such structures could occur on a subnanosecond time scale. The particles in the trimer are spherical, close to their thermodynamic equilibrium shape, suggesting that these structures could withstand relatively high temperatures without significant structural degradation. It should also be noted that the particle sizes and spacings simulated here are largely outside the regime where nonlocal and quantum effects start playing a significant role. The assumed gap size of 5 nm may be experimentally achieved using surface-charge-based binding or organic linker molecules, potentially enabling solution-based processing of large quantities of these photothermal plasmonic oligomers. The proposed structure

may be used for the generation of nanoscale bubbles, thermal radiation, the initiation of high-temperature chemical reactions in a low-temperature host, or even the realization of unusual material phases as a result of the expected rapid cooling of the central particle. The proposed approach is not limited to gold and silver, and may be extended to more complex nanoparticle oligomers.

IV. SUMMARY

In summary, we have presented a heterogeneous plasmonic trimer structure in which careful optimization of interparticle spacing enables the overlapping of plasmon resonances associated with the different materials in the trimer. The proposed structure enables significantly increased field enhancement factors and consequently efficient and localized heat generation. The relative absorption coefficient of a gold nanoparticle in a heterogeneous Ag-Au-Ag trimer was found to exceed that of isolated gold nanoparticles by two orders of magnitude. The structure potentially allows heterogeneous plasmonic trimers to be used in photothermal applications at significantly reduced laser irradiance, and may enable the investigation of thermally assisted effects on ultrashort time scales.

-
- [1] S. Lal, S. E. Clare, and N. J. Halas, *Acc. Chem. Res.* **41**, 1842 (2008).
- [2] X. H. Huang, P. K. Jain, I. H. El-Sayed, and M. A. El-Sayed, *Laser Med Sci.* **23**, 217 (2008).
- [3] C. M. Pitsillides, E. K. Joe, X. B. Wei, R. R. Anderson, and C. P. Lin, *Biophys. J.* **84**, 4023 (2003).
- [4] D. Lapotko, E. Lukianova, M. Potapnev, O. Aleinikova, and A. Oraevsky, *Cancer. Lett.* **239**, 36 (2006).
- [5] C. Loo, A. Lowery, N. J. Halas, J. West, and R. Drezek, *Nano Lett.* **5**, 709 (2005).
- [6] A. G. Skirtach, C. Dejugnat, D. Braun, A. S. Susha, A. L. Rogach, W. J. Parak, H. Mohwald, and G. B. Sukhorukov, *Nano Lett.* **5**, 1371 (2005).
- [7] B. P. Timko, T. Dvir, and D. S. Kohane, *Adv. Mater.* **22**, 4925 (2010).
- [8] A. S. Urban, T. Pfeiffer, M. Fedoruk, A. A. Lutich, and J. Feldmann, *ACS Nano* **5**, 3585 (2011).
- [9] D. Boyer, P. Tamarat, A. Maali, B. Lounis, and M. Orrit, *Science* **297**, 1160 (2002).
- [10] L. Cognet, C. Tardin, D. Boyer, D. Choquet, P. Tamarat, and B. Lounis, *Proc. Natl. Acad. Sci. USA* **100**, 11350 (2003).
- [11] L. Cognet, S. Berciaud, D. Lasne, and B. Lounis, *Anal. Chem.* **80**, 2288 (2008).
- [12] J. A. Copland, M. Eghtedari, V. L. Popov, N. Kotov, N. Mamedova, M. Motamedi, and A. A. Oraevsky, *Mol. Imaging Biol.* **6**, 341 (2004).
- [13] S. Mallidi, T. Larson, J. Aaron, K. Sokolov, and S. Emelianov, *Opt. Express* **15**, 6583 (2007).
- [14] A. Vogel, N. Linz, S. Freidank, and G. Paltauf, *Phys. Rev. Lett.* **100**, 038102 (2008).
- [15] E. Lukianova-Hleb, Y. Hu, L. Latterini, L. Tarpani, S. Lee, R. A. Drezek, J. H. Hafner, and D. O. Lapotko, *ACS Nano* **4**, 2109 (2010).
- [16] E. Y. Lukianova-Hleb, E. Sassaroli, A. Jones, and D. O. Lapotko, *Langmuir* **28**, 4858 (2012).
- [17] E. Boulais, R. Lachaine, and M. Meunier, *J. Phys. Chem. C* **117**, 9386 (2013).
- [18] E. Boulais, R. Lachaine, A. Hatef, and M. Meunier, *J. Photochem. Photobiol. C* **17**, 26 (2013).
- [19] O. Neumann, A. S. Urban, J. Day, S. Lal, P. Nordlander, and N. J. Halas, *ACS Nano* **7**, 42 (2013).
- [20] Z. Y. Fang, Y.-R. Zhen, O. Neumann, A. Polman, F. J. G. de Abajo, P. Nordlander, and N. J. Halas, *Nano Lett.* **13**, 1736 (2013).
- [21] L. Cao, D. N. Barsic, A. R. Guichard, and M. L. Brongersma, *Nano Lett.* **7**, 3523 (2007).
- [22] E. C. Garnett, W. S. Cai, J. J. Cha, F. Mahmood, S. T. Connor, M. G. Christoforo, Y. Cui, M. D. McGehee, and M. L. Brongersma, *Nat. Mater.* **11**, 241 (2012).
- [23] L. Liu, P. Peng, A. M. Hu, G. S. Zou, W. W. Duley, and Y. N. Zhou, *Appl. Phys. Lett.* **102**, 073107 (2013).
- [24] W. A. Challener *et al.*, *Nat. Photonics* **3**, 220 (2009).
- [25] G. L. Liu, J. Kim, Y. Lu, and L. P. Lee, *Nat. Mater.* **5**, 27 (2006).
- [26] J. S. Donner, G. Baffou, D. McCloskey, and R. Quidant, *ACS Nano* **5**, 5457 (2011).
- [27] K. Puech, F. Z. Henari, W. J. Blau, D. Duff, and G. Schmid, *Chem. Phys. Lett.* **247**, 13 (1995).
- [28] F. Hache, D. Ricard, C. Flytzanis, and U. Kreibig, *Appl. Phys. A: Mater. Sci. Process.* **47**, 347 (1988).
- [29] M. Perner, P. Bost, U. Lemmer, G. vonPlessen, J. Feldmann, U. Becker, M. Mennig, M. Schmitt, and H. Schmidt, *Phys. Rev. Lett.* **78**, 2192 (1997).
- [30] H. Inouye, K. Tanaka, I. Tanahashi, and K. Hirao, *Phys. Rev. B* **57**, 11334 (1998).
- [31] M. Rashidi-Huyeh and B. Palpant, *J. Appl. Phys.* **96**, 4475 (2004).

- [32] R. W. Schoenlein, W. Z. Lin, J. G. Fujimoto, and G. L. Eesley, *Phys. Rev. Lett.* **58**, 1680 (1987).
- [33] G. Bachelier, I. Russier-Antoine, E. Benichou, C. Jonin, N. Del Fatti, F. Vallee, and P. F. Brevet, *Phys. Rev. Lett.* **101**, 197401 (2008).
- [34] S. Sheikholeslami, Y. W. Jun, P. K. Jain, and A. P. Alivisatos, *Nano Lett.* **10**, 2655 (2010).
- [35] E. M. Larsson, C. Langhammer, I. Zoric, and B. Kasemo, *Science* **326**, 1091 (2009).
- [36] N. Liu, M. L. Tang, M. Hentschel, H. Giessen, and A. P. Alivisatos, *Nat. Mater.* **10**, 631 (2011).
- [37] T. Shegai, S. Chen, V. D. Miljković, G. Zengin, P. Johansson, and M. Käll, *Nat. Commun.* **2**, 481 (2011).
- [38] T. Shegai, P. Johansson, C. Langhammer, and M. Käll, *Nano Lett.* **12**, 2464 (2012).
- [39] K. Li, M. I. Stockman, and D. J. Bergman, *Phys. Rev. Lett.* **91**, 227402 (2003).
- [40] P. Nordlander, C. Oubre, E. Prodan, K. Li, and M. I. Stockman, *Nano Lett.* **4**, 899 (2004).
- [41] S. Toroghi and P. G. Kik, *Appl. Phys. Lett.* **100**, 183105 (2012).
- [42] *Microwave Studio, Computer Simulation Technology*, Darmstadt, Germany, 2012.
- [43] S. Toroghi and P. G. Kik, *Phys. Rev. B* **85**, 045432 (2012).
- [44] P. B. Johnson and R. W. Christy, *Phys. Rev. B* **6**, 4370 (1972).
- [45] M. Hu and G. V. Hartland, *J. Phys. Chem. B* **106**, 7029 (2002).